Oscillation effect and sign-change behaviour of the bias-dependent tunnelling magnetoresistance in ferromagnetic junctions

2005 J. Phys.: Condens. Matter 17 4121

(http://iopscience.iop.org/0953-8984/17/26/011)

INSTITUTE OF PHYSICS PUBLISHING JOURNAL OF PHYSICS: CONDENSED MATTER

J. Phys.: Condens. Matter **17** (2005) 4121–4134 doi:10.1088/0953-8984/17/26/011

Oscillation effect and sign-change behaviour of the bias-dependent tunnelling magnetoresistance in ferromagnetic junctions

Yuan Ren, Zheng-zhong Li, Ming-wen Xiao and An Hu

Department of Physics, Nanjing University, Nanjing 210093, People's Republic of China

E-mail: zligong@nju.edu.cn

Received 25 January 2005, in final form 22 March 2005
Published 17 June 2005
Online at stacks.iop.org/JPhysCM/17/4121

Abstract

In this paper, we present a spintronic tunnelling theory for ferromagnet/insulator/ferromagnet (FM/I/FM) junctions. With the use of Airy functions, it can analytically account for both the low-bias and the high-bias tunnelling magnetoresistances (TMRs). We find that the sign-change behaviour of TMR can only occur in the low-bias region, due to the quantum coherence in FM/I/FM junctions. In the high-bias region, the TMR will oscillate between positive and negative with increasing bias voltage. Physically, this oscillation arises from the interference between the incident and reflected electron waves in the barrier region. The effects of the barrier height, the barrier width and the electron effective mass in the barrier are studied systematically. The theoretical results obtained from the exact Airy functions agree well with TMR experiments on Ta_2O_5- and Al_2O_3-barrier junctions, within the whole measurable range of bias voltage.

1. Introduction

Tunnelling magnetoresistance (TMR) in ferromagnet/insulator/ferromagnet (FM/I/FM) junctions was first studied theoretically and observed experimentally by Jullière [1] in 1975. Now, it attracts intensive attention because of its great potential in information technology. For real applications, it is very important to know the bias dependence of TMR. Early experimental studies were limited within a small range of bias. In 1999, Sharma *et al* [2] fabricated Ta_2O_5-barrier junctions and began an experimental investigation of the bias dependence of TMR within a widened range of bias. As a result, two new features have been found within the measurable range of the applied voltage[1]. One is that, as the bias voltage is increased, the TMR decreases rapidly and changes its sign from positive to negative at a finite voltage. The

[1] Beyond this range, the dielectric oxide barrier will be broken down due to the smallness of the barrier thickness and its resulting strong electric field.

other is that, when the bias voltage is further increased, the TMR becomes concave-up with a tail bending upwards with the increase of the applied voltage (see figure 2 in [2]). The second feature reminds us that the tail may be a physical symbol that the TMR would be oscillatory if the bias voltage went out of the measurable range of the applied voltage. In addition, a junction with an Al_2O_3 barrier shows [2] that the TMR decreases monotonically with the increase of bias voltage but remains positive before the breakdown of the junction, which implies that the measurable range of bias voltage for the Al_2O_3-barrier junction lies in such a low-bias region that the sign change and oscillation could not be observed, in comparison to the Ta_2O_5-barrier junction.

In order to interpret the experiments, we have developed a theory [3], by extending the Slonczewski model [4] from the zero-bias case to the low-bias case. In this theory, the single-electron potential is assumed to be trapezoidal within the barrier region, and the tunnelling electron is described approximately by the Wentzel–Kramers–Brillouin (WKB) wavefunction. Upon matching the WKB wavefunction quantum-mechanically with the wavefunctions of the two FM electrodes at the two interfaces, we find that the sign-change behaviour of TMR originates from the quantum coherence in the FM/I/FM system [3]. Although our previous work [3] succeeds in explaining the sign change of TMR, it cannot explain the concavity or oscillation of TMR at the high-bias voltage. In addition, the numerical calculation performed by Montaigne *et al* [5] shows an oscillatory TMR within the high-bias regime. However, this kind of numerical method is not convenient for revealing the physical mechanism responsible for the oscillation of TMR.

The purpose of this paper is to study the physical mechanism for the oscillation of TMR in FM/I/FM junctions analytically. To this end, we will establish a unified spintronic tunnelling theory suitable not only for the low-bias region but also for the high-bias region.

The rest of the paper is organized as follows. In section 2, we present the spintronic tunnelling model for the FM/I/FM junction, and derive the exact transmission coefficients and TMR for the case of a finite applied voltage. In section 3, we study in an analytical manner the mechanisms for the sign change and oscillation of TMR, then discuss the influences of the barrier height, barrier width and electron effective mass on the oscillation of TMR, and then qualitatively compare the theoretical results with the experiments. Finally, a brief summary will be given in section 4.

2. Spintronic tunnelling model

Following previous work [3, 6–8], we adopt the free electron model with parabolic bands for the three regions of the FM/I/FM system. As usual, the energy zero is selected at the centre of the exchange splitting of the left electrode. Therefore, the system considered can be described by the spintronic tunnelling model as follows:

$$H_{\mathrm{L}} = -\frac{\hbar^2}{2m}\nabla^2 - \sigma_{\mathrm{L}}\Delta + \phi\,(x)\,, \qquad (x \leqslant 0)\,, \tag{1}$$

$$H_{\mathrm{B}} = -\frac{\hbar^2}{2m_{\mathrm{B}}}\nabla^2 + \phi\,(x)\,, \qquad (0 < x < d)\,, \tag{2}$$

$$H_{\mathrm{R}} = -\frac{\hbar^2}{2m}\nabla^2 - \sigma_{\mathrm{R}}\Delta + \phi\,(x)\,, \qquad (x \geqslant d)\,, \tag{3}$$

where H_{L}, H_{R} and H_{B} are the longitudinal parts of the Hamiltonians for the left and right electrodes and the barrier, respectively; Δ is the half exchange splitting between the two spin bands of the ferromagnetic electrodes (the two electrodes are supposed to be made of identical ferromagnetic material); m and m_{B} are the effective masses of the electrons in the electrodes and barrier; $\sigma_{\mathrm{L(R)}} = \pm 1$ denote respectively the up- and down-spin states of the electrons in

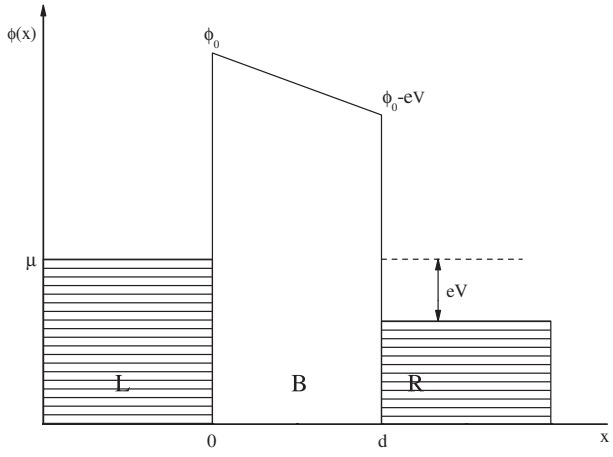

Figure 1. A schematic potential for the ferromagnetic junction under the bias $V > 0$.

the left (right) ferromagnetic electrode (the magnetizations of the two electrodes are parallel if $\sigma_{\mathrm{L}} = \sigma_{\mathrm{R}}$, and antiparallel if $\sigma_{\mathrm{L}} = -\sigma_{\mathrm{R}}$); and $\phi(x)$ represents the single-particle potential,

$$\phi(x) = \begin{cases} 0, & x < 0 \\ \phi_0 - \dfrac{x}{d}eV, & 0 \leqslant x \leqslant d \\ -eV, & x > d, \end{cases} \tag{4}$$

with V being the bias voltage, ϕ_0 the barrier height without any bias voltage, and d the barrier width. The potential $\phi(x)$ is shown schematically in figure 1.

Obviously, the potential $\phi(x)$ within the left or right FM electrode ($x < 0$ or $x > d$) is constant and independent of the longitudinal coordinates x. Therefore, the wavefunctions within the two ferromagnetic electrodes are simply plane waves,

$$\psi_{\sigma_{\mathrm{L}}}(x) = k_{\sigma_{\mathrm{L}}}^{-1/2}(\mathrm{e}^{\mathrm{i}k_{\sigma_{\mathrm{L}}}x} + R_{\sigma_{\mathrm{L}}}\mathrm{e}^{-\mathrm{i}k_{\sigma_{\mathrm{L}}}x}), \qquad (x \leqslant 0), \tag{5}$$

$$\psi_{\sigma_{\mathrm{R}}}(x) = k_{\sigma_{\mathrm{R}}}^{-1/2}C_{\sigma_{\mathrm{R}}}\mathrm{e}^{\mathrm{i}k_{\sigma_{\mathrm{R}}}(x-d)}, \qquad (x \geqslant d), \tag{6}$$

where

$$k_{\sigma_{\mathrm{L}}} = \left(\frac{2m}{\hbar^2}\right)^{1/2}\sqrt{E_x^{\mathrm{L}} + \sigma_{\mathrm{L}}\Delta}, \tag{7}$$

$$k_{\sigma_{\mathrm{R}}} = \left(\frac{2m}{\hbar^2}\right)^{1/2}\sqrt{E_x^{\mathrm{R}} + eV + \sigma_{\mathrm{R}}\Delta}. \tag{8}$$

Here E_x^{L} and E_x^{R} stand for the longitudinal part of the electron energy in the left and right electrodes, respectively.

As regards the barrier region, the potential $\phi(x)$ is a linear function of x, or of trapezoidal shape, the exact wavefunction must be expressed in terms of the Airy functions $\mathrm{Ai}(z)$ and $\mathrm{Bi}(z)$,

$$\psi_{\mathrm{B}}(x) = a \cdot \mathrm{Ai}(z) + b \cdot \mathrm{Bi}(z), \tag{9}$$

where a and b are the coefficients which should be determined by quantum-mechanical matching, and

$$z = -z'\left(x + \frac{E_x^{\mathrm{B}} - \phi_0}{eV}d\right), \tag{10}$$

$$z' = \left(\frac{2m_{\mathrm{B}}eV}{\hbar^2 d}\right)^{\frac{1}{3}}. \tag{11}$$

Here E_x^{B} is the longitudinal part of the electron energy within the barrier region.

Because of energy conservation and the conservation of the lateral momentum, the longitudinal energies E_x^{L}, E_x^{R} and E_x^{B} appearing in equations (7), (8) and (10) are not independent of each other; they satisfy the relations [9]

$$E_x^{\mathrm{B}} = E_x^{\mathrm{L}} + E_t^{\mathrm{L}}\left(1 - \frac{m}{m_{\mathrm{B}}}\right), \tag{12}$$

$$E_x^{\mathrm{R}} = E_x^{\mathrm{L}}, \tag{13}$$

where E_t^{L} is the lateral part of the electron energy. Equation (13) is obtained simply because the two electrodes are assumed to have the same electron effective masses.

It should be pointed out that the solution of equation (9) is always valid no matter how large the bias voltage V is, i.e., equation (9) is appropriate for both the low- and high-bias regions. We shall see in the following section that the $\psi_{\mathrm{B}}(x)$ can be approximated by the WKB wavefunction in the low-bias region, which is the case we considered in [3, 6–8]. If the bias voltage becomes high, there will arise a turning point in the barrier region, the WKB approximation for $\psi_{\mathrm{B}}(x)$ is no longer valid, and a qualitative analysis must be done carefully. That is just the case in which we are interested in this paper.

After quantum-mechanical matching of the wavefunctions $\psi_{\sigma_{\mathrm{L}}}(x)$, $\psi_{\sigma_{\mathrm{R}}}(x)$ and $\psi_{\mathrm{B}}(x)$ at $x = 0$ and d, the transmission coefficient $T_{\sigma_{\mathrm{L}}\sigma_{\mathrm{R}}}$ can be obtained as follows:

$$\begin{aligned} T_{\sigma_{\mathrm{L}}\sigma_{\mathrm{R}}} = \frac{4\widetilde{k}_{\sigma_{\mathrm{R}}}}{\pi^2\widetilde{k}_{\sigma_{\mathrm{L}}}}\Bigg\{\Bigg[&(\mathrm{Ai}(z_0)\mathrm{Bi}'(z_{\mathrm{d}}) - \mathrm{Ai}'(z_{\mathrm{d}})\mathrm{Bi}(z_0)) \\ &+ \frac{\widetilde{k}_{\sigma_{\mathrm{R}}}}{\widetilde{k}_{\sigma_{\mathrm{L}}}}(\mathrm{Ai}(z_{\mathrm{d}})\mathrm{Bi}'(z_0) - \mathrm{Ai}'(z_0)\mathrm{Bi}(z_{\mathrm{d}}))\Bigg]^2 \\ &+ \Bigg[\frac{\widetilde{k}_{\sigma_{\mathrm{R}}}}{\widetilde{z}'}(\mathrm{Ai}(z_0)\mathrm{Bi}(z_{\mathrm{d}}) - \mathrm{Ai}(z_{\mathrm{d}})\mathrm{Bi}(z_0)) \\ &+ \frac{\widetilde{z}'}{\widetilde{k}_{\sigma_{\mathrm{L}}}}(\mathrm{Ai}'(z_0)\mathrm{Bi}'(z_{\mathrm{d}}) - \mathrm{Ai}'(z_{\mathrm{d}})\mathrm{Bi}'(z_0))\Bigg]^2\Bigg\}^{-1}, \end{aligned} \tag{14}$$

where

$$\widetilde{k}_{\sigma_{\mathrm{L}}} = \frac{k_{\sigma_{\mathrm{L}}}}{m}, \tag{15}$$

$$\widetilde{k}_{\sigma_{\mathrm{R}}} = \frac{k_{\sigma_{\mathrm{R}}}}{m}, \tag{16}$$

$$\widetilde{z}' = \frac{z'}{m_{\mathrm{B}}}, \tag{17}$$

$$z_0 = z(E_x^{\mathrm{B}}, V, 0) = z'\frac{\phi_0 - E_x^{\mathrm{B}}}{eV}d, \tag{18}$$

$$z_{\mathrm{d}} = z(E_x^{\mathrm{B}}, V, d) = z'\frac{\phi_0 - (E_x^{\mathrm{B}} + eV)}{eV}d. \tag{19}$$

If the two electrodes are paramagnetic, the transmission coefficient $T_{\sigma_{\mathrm{L}}\sigma_{\mathrm{R}}}$ will automatically reduce to the exact result [10] derived historically first by Gundlach.

It is worth noting that the transmission coefficient $T_{\sigma_{\mathrm{L}}\sigma_{\mathrm{R}}}$ of equation (14) is a rigorous solution to the spintronic tunnelling model of equations (1)–(3), because $\psi_{\sigma_{\mathrm{L}}}(x)$, $\psi_{\sigma_{\mathrm{R}}}(x)$ and $\psi_{\mathrm{B}}(x)$ are all exact wavefunctions, and their connections at both $x = 0$ and d are fully quantum-mechanical matched.

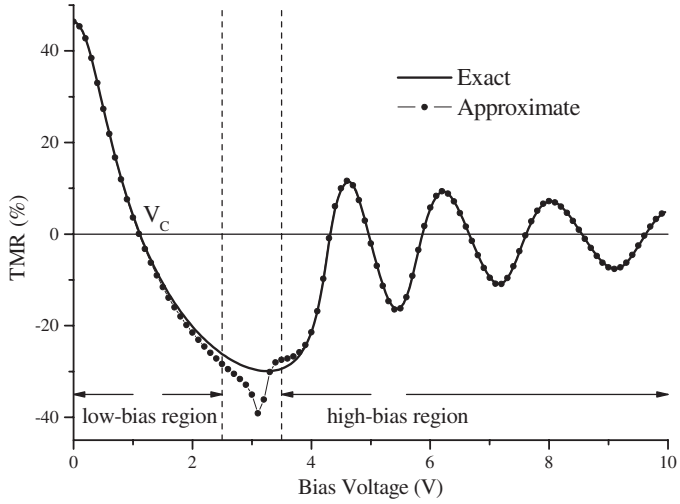

Figure 2. The comparison between the approximate TMR and the exact TMR. The calculating parameters are $E_{F\uparrow} = 5eV$, $m_B/m = 1$, $k_{F\downarrow}/k_{F\uparrow} = 0.22$, $d = 20$ Å, $\kappa_F^2/\kappa_{F\uparrow}^2 = 0.6$.

With the rigorous transmission coefficient $T_{\sigma_L\sigma_R}$ given above, the tunnelling current densities can be expressed as [11]

$$J_P(V) = \frac{em}{4\pi^2\hbar^3}\int dE_x^L \int dE_t^L \,(T_{\uparrow\uparrow} + T_{\downarrow\downarrow})\left[f(E_x^L + E_t^L) - f(E_x^L + E_t^L + eV)\right], \tag{20}$$

$$J_{AP}(V) = \frac{em}{4\pi^2\hbar^3}\int dE_x^L \int dE_t^L \,(T_{\uparrow\downarrow} + T_{\downarrow\uparrow})\left[f(E_x^L + E_t^L) - f(E_x^L + E_t^L + eV)\right], \tag{21}$$

where the subscripts P and AP refer to parallel and antiparallel configurations of the two FM electrodes, respectively.

Usually, the TMR is defined as

$$\text{TMR} \equiv \frac{J_P(V) - J_{AP}(V)}{J_P(V)} = \frac{\Delta J(V)}{J_P(V)}, \tag{22}$$

which can be calculated from equations (20) and (21).

Up to now, a spintronic tunnelling theory for the FM/I/FM system has been established; obviously, it is not only suitable for the low-bias region but also suitable for the high-bias region.

3. Numerical results and discussions

By using equations (14), (20)–(22), a numerical calculation can be performed. Similarly to our previous works [3, 8], we choose $E_{F\uparrow}$, $\kappa_F^2/k_{F\uparrow}^2$, $k_{F\downarrow}/k_{F\uparrow}$, d and m_B/m as the physical parameters. Here, $E_{F\uparrow}$ denotes the Fermi energy of the spin-up electrons in the FM electrodes; $\kappa_F^2/k_{F\uparrow}^2 = (\phi_0 - \mu)/E_{F\uparrow}$ the relative barrier height to the chemical potential μ; $k_{F\downarrow}/k_{F\uparrow}$ the ratio of the Fermi wavenumbers for different spin bands. Hereafter, we will consider only the zero-temperature case and a thick barrier junction. The results are shown by the solid curve in figure 2. One can easily see that, as the bias voltage increases, the TMR first decreases rapidly, then changes its sign from positive to negative at a critical voltage V_c, and then bends upwards and begins to oscillate. This is in agreement with the TMR experiments on the Ta_2O_5-barrier junction; in particular, it reproduces the two new features of TMR: the sign change within the low-bias region and the oscillation within the high-bias region.

Now, we turn to analyse in detail the physical mechanisms responsible for the sign change and oscillation of TMR. To this end, we shall follow Gundlach [10] and Duke [11] to define two

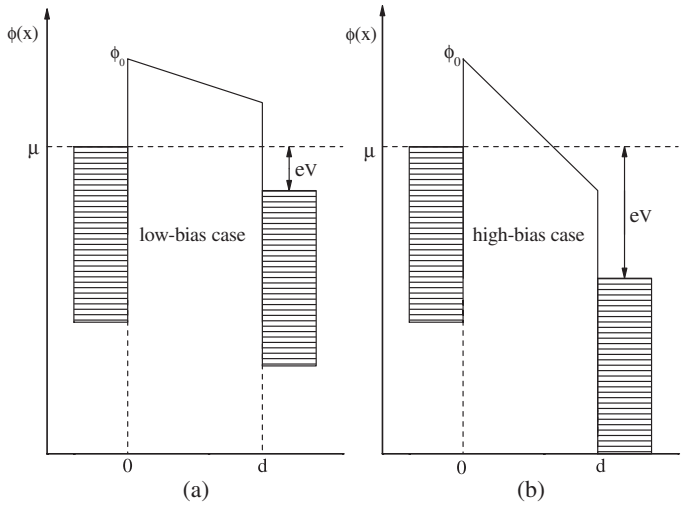

Figure 3. Schematic illustration for (a): the low-bias case and (b): the high-bias case.

regions according to the magnitude of the bias voltage: the low-bias region and the high-bias region. As can be seen later, the TMR will show quite different behaviours in these two regions.

3.1. The low-bias region

In this region, the Fermi level is far below from the barrier height: $\phi_0 - \mu \gg 0$, and the bias voltage is quite small: $eV \ll \phi_0 - \mu$, which is schematically depicted in figure 3(a). Mathematically, this is equivalent to $z_0 \gg 1$ and $z_\mathrm{d} \gg 1$. In such a case, $z \gg 1$, the Airy functions can be approximated as [12]

$$\mathrm{Ai}(z) = \tfrac{1}{2}\pi^{-\frac{1}{2}} z^{-\frac{1}{4}} \mathrm{e}^{-\gamma}, \tag{23}$$

$$\mathrm{Bi}(z) = \pi^{-\frac{1}{2}} z^{-\frac{1}{4}} \mathrm{e}^{\gamma}, \tag{24}$$

$$\mathrm{Ai}'(z) = -\tfrac{1}{2}\pi^{-\frac{1}{2}} z^{\frac{1}{4}} \mathrm{e}^{-\gamma}, \tag{25}$$

$$\mathrm{Bi}'(z) = \pi^{-\frac{1}{2}} z^{\frac{1}{4}} \mathrm{e}^{\gamma}, \tag{26}$$

where

$$\gamma = \frac{2}{3} z^{\frac{3}{2}}. \tag{27}$$

Note that, when $z \gg 1$, $\mathrm{Ai}(z)$ and $\mathrm{Ai}'(z)$ are exponentially decreasing functions of z, whereas $\mathrm{Bi}(z)$ and $\mathrm{Bi}'(z)$ the exponentially increasing functions of z.

Inserting equations (23)–(26) into equation (14), one has

$$T_{\sigma_\mathrm{L}\sigma_\mathrm{R}} = \frac{16 \widetilde{k}_{\sigma_\mathrm{L}} \widetilde{k}_{\sigma_\mathrm{R}} \widetilde{\kappa}_\mathrm{L} \widetilde{\kappa}_\mathrm{R}}{\left(\widetilde{\kappa}_\mathrm{L}^2 + \widetilde{k}_{\sigma_\mathrm{L}}^2\right)\left(\widetilde{\kappa}_\mathrm{R}^2 + \widetilde{k}_{\sigma_\mathrm{R}}^2\right)} \mathrm{e}^{-2\int_0^d \widetilde{\kappa}\,\mathrm{d}x}, \tag{28}$$

where

$$\widetilde{\kappa}_\mathrm{L} = \widetilde{\kappa}(E_x^\mathrm{B}, 0, V) = \frac{1}{m_\mathrm{B}} \left(\frac{2m_\mathrm{B}}{\hbar^2}\right)^{1/2} \left(\phi_0 - E_x^\mathrm{B}\right)^{1/2}, \tag{29}$$

$$\widetilde{\kappa}_\mathrm{R} = \widetilde{\kappa}(E_x^\mathrm{B}, d, V) = \frac{1}{m_\mathrm{B}} \left(\frac{2m_\mathrm{B}}{\hbar^2}\right)^{1/2} \left(\phi_0 - eV - E_x^\mathrm{B}\right)^{1/2}, \tag{30}$$

$$\widetilde{\kappa} = \widetilde{\kappa}(E_x^\mathrm{B}, x, V) = \frac{1}{m_\mathrm{B}} \left(\frac{2m_\mathrm{B}}{\hbar^2}\right)^{1/2} \left(\phi_0 - \frac{x}{d} eV - E_x^\mathrm{B}\right)^{1/2}. \tag{31}$$

In deriving equation (28) we have used the relation

$$\int_0^d \widetilde{\kappa}\,\mathrm{d}x = \tfrac{2}{3}\left(z_0^{3/2} - z_\mathrm{d}^{3/2}\right) \gg 1, \tag{32}$$

because, as mentioned above, the barrier width is rather thick.

We can now calculate the approximate TMR from equations (20)–(22) and (28); this is shown by the dotted curve in figure 2. Clearly, the approximate result is in good agreement with the exact one (the solid curve) within the low-bias range. This demonstrates that the above approximation is quite accurate and is thus suitable for discussing the sign-change mechanism of TMR in the low-bias region. That can be done as follows.

We can obtain from equations (20), (21) and (28) that

$$\Delta J(V) = \frac{em}{4\pi^2\hbar^3}\int \mathrm{d}E_x^\mathrm{L}\int \mathrm{d}E_t^\mathrm{L} A(E_x^\mathrm{L}, E_t^\mathrm{L}, V) D(E_x^\mathrm{L}, E_t^\mathrm{L}, V) \times \exp\left(-2\int_0^d \widetilde{\kappa}\,\mathrm{d}x\right)\left[f(E_x^\mathrm{L}+E_t^\mathrm{L}) - f(E_x^\mathrm{L}+E_t^\mathrm{L}+eV)\right], \tag{33}$$

where

$$A(E_x^\mathrm{L}, E_t^\mathrm{L}, V) = \frac{4\widetilde{\kappa}_\mathrm{L}\left(\widetilde{k}_{\mathrm{L}\uparrow} - \widetilde{k}_{\mathrm{L}\downarrow}\right)\left(\widetilde{\kappa}_\mathrm{L}^2 - \widetilde{k}_{\mathrm{L}\uparrow}\widetilde{k}_{\mathrm{L}\downarrow}\right)}{\left(\widetilde{\kappa}_\mathrm{L}^2 + \widetilde{k}_{\mathrm{L}\uparrow}^2\right)\left(\widetilde{\kappa}_\mathrm{L}^2 + \widetilde{k}_{\mathrm{L}\downarrow}^2\right)} \cdot \frac{4\widetilde{\kappa}_\mathrm{R}\left(\widetilde{k}_{\mathrm{R}\uparrow} - \widetilde{k}_{\mathrm{R}\downarrow}\right)}{\left(\widetilde{\kappa}_\mathrm{R}^2 + \widetilde{k}_{\mathrm{R}\uparrow}^2\right)\left(\widetilde{\kappa}_\mathrm{R}^2 + \widetilde{k}_{\mathrm{R}\downarrow}^2\right)}, \tag{34}$$

$$D(E_x^\mathrm{L}, E_t^\mathrm{L}, V) = \widetilde{\kappa}_\mathrm{R}^2 - \widetilde{k}_{\mathrm{R}\uparrow}\widetilde{k}_{\mathrm{R}\downarrow}. \tag{35}$$

From equations (15), (16), (29) and (30), it is easy to show that $A(E_x^\mathrm{L}, E_t^\mathrm{L}, V) > 0$, i.e. $A(E_x^\mathrm{L}, E_t^\mathrm{L}, V)$ does not change sign with V [3, 6, 8]. By substituting equations (16) and (30) into (35), the quantum-coherence factor $D(E_x^\mathrm{L}, E_t^\mathrm{L}, V)$ becomes

$$D(E_x^\mathrm{L}, E_t^\mathrm{L}, V) = \frac{2}{m_\mathrm{B}\hbar^2}\left[\phi_0 + E_t^\mathrm{L}\left(\frac{m}{m_\mathrm{B}} - 1\right) - \left(eV + E_x^\mathrm{L}\right)\right] - \frac{2}{m\hbar^2}\sqrt{(E_x^\mathrm{L}+eV)^2 - \Delta^2}, \tag{36}$$

which is a rapidly decreasing function of V, and will become negative when the bias goes beyond the critical voltage V_c. That is the reason why the TMR decreases and changes in sign within the low-bias range [3, 6, 8].

Setting $m_\mathrm{B} = m$, the longitudinal part of the electron energy E_x^L, E_x^B and E_x^R can be simply written as E_x. Therefore, equation (28) reduces to

$$T_{\sigma_\mathrm{L}\sigma_\mathrm{R}} = \frac{16k_{\sigma_\mathrm{L}}k_{\sigma_\mathrm{R}}\kappa_\mathrm{L}\kappa_\mathrm{R}}{\left(\kappa_\mathrm{L}^2 + k_{\sigma_\mathrm{L}}^2\right)\left(\kappa_\mathrm{R}^2 + k_{\sigma_\mathrm{R}}^2\right)}\mathrm{e}^{-2\int_0^d \kappa\,\mathrm{d}x}, \tag{37}$$

where

$$\kappa_\mathrm{L} = \left(\frac{2m}{\hbar^2}\right)^{1/2}(\phi_0 - E_x)^{1/2}, \tag{38}$$

$$\kappa_\mathrm{R} = \left(\frac{2m}{\hbar^2}\right)^{1/2}(\phi_0 - eV - E_x)^{1/2}, \tag{39}$$

$$\kappa = \left(\frac{2m}{\hbar^2}\right)^{1/2}\left(\phi_0 - \frac{x}{d}eV - E_x\right)^{1/2}. \tag{40}$$

Equation (37) is just the transmission coefficient given in [3, 6], from which the other results thereof can also be reproduced identically. In other words, the results of [3, 6] can be derived again from the present rigorous solution of equation (14); this proves that the adoption of the WKB approximation for $\psi_\mathrm{B}(x)$ in [3, 6] is rational and completely appropriate for the low-bias region.

3.2. The high-bias region

In this region, the Fermi level is also far below from the barrier height: $\phi_0 - \mu \gg 0$, but the bias voltage is quite large: $eV \gg \phi_0 - \mu$, which is schematically depicted in figure 3(b). This means that $z_0 \gg 1$ but $z_d \ll -1$. For $z \ll -1$, the Airy functions must, instead of equations (23)–(26), be approximated as [12]

$$\mathrm{Ai}(z) = \pi^{-\frac{1}{2}} |z|^{-\frac{1}{4}} \sin\left(\gamma + \frac{\pi}{4}\right), \tag{41}$$

$$\mathrm{Bi}(z) = \pi^{-\frac{1}{2}} |z|^{-\frac{1}{4}} \cos\left(\gamma + \frac{\pi}{4}\right), \tag{42}$$

$$\mathrm{Ai}'(z) = -\pi^{-\frac{1}{2}} |z|^{\frac{1}{4}} \cos\left(\gamma + \frac{\pi}{4}\right), \tag{43}$$

$$\mathrm{Bi}'(z) = \pi^{-\frac{1}{2}} |z|^{\frac{1}{4}} \sin\left(\gamma + \frac{\pi}{4}\right), \tag{44}$$

where

$$\gamma = \tfrac{2}{3} |z|^{\frac{3}{2}}. \tag{45}$$

Apparently, $\mathrm{Ai}(z)$, $\mathrm{Bi}(z)$, $\mathrm{Ai}'(z)$ and $\mathrm{Bi}'(z)$ are all oscillating functions of z when $z \ll -1$, which is basically distinct from the case of $z \gg 1$ giving in equations (23)–(26).

Substituting equations (23)–(26) and (41)–(44) into equation (14) respectively for the points $z = z_0$ and z_d, one has

$$T_{\sigma_L \sigma_R} = \frac{8\widetilde{k}_{\sigma_L} \widetilde{k}_{\sigma_R} \widetilde{\kappa}_L \widetilde{k}_d}{\left(\widetilde{\kappa}_L^2 + \widetilde{k}_{\sigma_L}^2\right)\left[\widetilde{k}_d^2 + \widetilde{k}_{\sigma_R}^2 + (\widetilde{k}_d^2 - \widetilde{k}_{\sigma_R}^2)\sin(2\gamma_d)\right]} \mathrm{e}^{-2\gamma_0}, \tag{46}$$

where

$$\widetilde{k}_d = \frac{1}{m_B}\left(\frac{2m_B}{\hbar^2}\right)^{1/2} \left(E_x^B - \phi_0 + eV\right)^{1/2}, \tag{47}$$

$$\gamma_0 = \frac{2(2m_B/\hbar^2)^{1/2} d}{3eV} \left(\phi_0 - E_x^B\right)^{3/2}, \tag{48}$$

$$\gamma_d = \frac{2(2m_B/\hbar^2)^{1/2} d}{3eV} \left(E_x^B + eV - \phi_0\right)^{3/2}. \tag{49}$$

Using equation (46), the approximate TMR can be calculated; the results are shown by the dotted curve within the high-bias region in figure 2. Obviously, in this region the approximate and the exact curves still agree very well. The approximation supplies us with a convenient tool to analyse the mechanism for the oscillation of TMR occurring in the high-bias regime.

In analogy to the low-bias region, we can, with the help of equation (46), reformulate ΔJ as

$$\Delta J = \frac{em}{4\pi^2\hbar^3} \int \mathrm{d}E_x^L \int \mathrm{d}E_t^L \, B(E_x^L, E_t^L, V) C(E_x^L, E_t^L, V) \times \exp(-2\gamma_0)\left[f(E_x^L + E_t^L) - f(E_x^L + E_t^L + eV)\right], \tag{50}$$

where

$$B(E_x^L, E_t^L, V) = \frac{8\widetilde{\kappa}_L(\widetilde{k}_{L\uparrow} - \widetilde{k}_{L\downarrow})(\widetilde{\kappa}_L^2 - \widetilde{k}_{L\uparrow}\widetilde{k}_{L\downarrow})}{(\widetilde{\kappa}_L^2 + \widetilde{k}_{L\uparrow}^2)(\widetilde{\kappa}_L^2 + \widetilde{k}_{L\downarrow}^2)} \times \frac{\widetilde{k}_d(\widetilde{k}_{R\uparrow} - \widetilde{k}_{R\downarrow})(\widetilde{k}_d^2 + \widetilde{k}_{R\uparrow}\widetilde{k}_{R\downarrow})}{[\widetilde{k}_d^2 + \widetilde{k}_{R\uparrow}^2 + (\widetilde{k}_d^2 - \widetilde{k}_{R\uparrow}^2)\sin(2\gamma_d)][\widetilde{k}_d^2 + \widetilde{k}_{R\downarrow}^2 + (\widetilde{k}_d^2 - \widetilde{k}_{R\downarrow}^2)\sin(2\gamma_d)]}, \tag{51}$$

$$C(E_x^{\mathrm{L}}, E_t^{\mathrm{L}}, V) = \frac{\widetilde{k}_{\mathrm{d}}^2 - \widetilde{k}_{\mathrm{R}\uparrow}\widetilde{k}_{\mathrm{R}\downarrow}}{\widetilde{k}_{\mathrm{d}}^2 + \widetilde{k}_{\mathrm{R}\uparrow}\widetilde{k}_{\mathrm{R}\downarrow}} - \sin(2\gamma_{\mathrm{d}}). \tag{52}$$

From equations (15) and (16), we have

$$\widetilde{k}_{\mathrm{L}\uparrow} - \widetilde{k}_{\mathrm{L}\downarrow} = \frac{1}{m}\left(\frac{2m}{\hbar^2}\right)^{1/2}\left[\sqrt{E_x^{\mathrm{L}} + \Delta} - \sqrt{E_x^{\mathrm{L}} - \Delta}\right] > 0, \tag{53}$$

$$\widetilde{k}_{\mathrm{R}\uparrow} - \widetilde{k}_{\mathrm{R}\downarrow} = \frac{1}{m}\left(\frac{2m}{\hbar^2}\right)^{1/2}\left[\sqrt{E_x^{\mathrm{L}} + eV + \Delta} - \sqrt{E_x^{\mathrm{L}} + eV - \Delta}\right] > 0. \tag{54}$$

The inequalities (53) and (54) are satisfied because the spin-up band has been assumed to be the majority band. As is the usual case for experimental FM metals, the effective polarization of the FM electrode [4],

$$P_{\mathrm{eff}} = \frac{(k_\uparrow - k_\downarrow)}{(k_\uparrow + k_\downarrow)} \cdot \frac{(\kappa^2 - k_\uparrow k_\downarrow)}{(\kappa^2 + k_\uparrow k_\downarrow)}, \tag{55}$$

is chosen to be positive, and thus we have $\kappa_{\mathrm{L}}^2 - k_{\mathrm{L}\uparrow}k_{\mathrm{L}\downarrow} > 0$. This implies that

$$\kappa_{\mathrm{L}}^2 - \frac{m_{\mathrm{B}}}{m}k_{\mathrm{L}\uparrow}k_{\mathrm{L}\downarrow} > 0, \tag{56}$$

when $m_{\mathrm{B}}/m < 1$. Therefore, from equations (7), (15), (29) and (38), one finds

$$\widetilde{\kappa}_{\mathrm{L}}^2 - \widetilde{k}_{\mathrm{L}\uparrow}\widetilde{k}_{\mathrm{L}\downarrow} = \frac{1}{m_{\mathrm{B}}m}\left(\kappa_{\mathrm{L}}^2 - \frac{m_{\mathrm{B}}}{m}k_{\mathrm{L}\uparrow}k_{\mathrm{L}\downarrow}\right) > 0. \tag{57}$$

Combining equations (53), (54) and (57) results in

$$B(E_x^{\mathrm{L}}, E_t^{\mathrm{L}}, V) > 0, \tag{58}$$

that is to say, the factor $B(E_x^{\mathrm{L}}, E_t^{\mathrm{L}}, V)$ is always positive regardless of the magnitude of the bias voltage. As for the factor $C(E_x^{\mathrm{L}}, E_t^{\mathrm{L}}, V)$, observing

$$-1 \leqslant \sin(2\gamma_{\mathrm{d}}) \leqslant 1, \tag{59}$$

$$-1 < \frac{\widetilde{k}_{\mathrm{d}}^2 - \widetilde{k}_{\mathrm{R}\uparrow}\widetilde{k}_{\mathrm{R}\downarrow}}{\widetilde{k}_{\mathrm{d}}^2 + \widetilde{k}_{\mathrm{R}\uparrow}\widetilde{k}_{\mathrm{R}\downarrow}} < 1, \tag{60}$$

one can see from equation (52) that the sign of $C(E_x^{\mathrm{L}}, E_t^{\mathrm{L}}, V)$ will change with γ_{d}. According to equation (49), γ_{d} is a function of V. Therefore, the factor $C(E_x^{\mathrm{L}}, E_t^{\mathrm{L}}, V)$, being a sine function of γ_{d}, will oscillate between positive and negative values sinusoidally with increasing bias voltage. As a combined result of $B(E_x^{\mathrm{L}}, E_t^{\mathrm{L}}, V)$ and $C(E_x^{\mathrm{L}}, E_t^{\mathrm{L}}, V)$, ΔJ and consequently the TMR of equation (22) will oscillate with increasing applied voltage. That is the microscopic reason for the oscillation effect of TMR in the high-bias region. Physically, if the bias voltage (eV) is larger than the barrier height ($\phi_0 - \mu$), the electrons near the Fermi level will enter into the conduction band of the barrier and then be reflected by the right electrode–barrier interface. It is just this interference between the incident and reflected waves that is microscopically responsible for the oscillation of TMR within the high-bias region. This oscillation cannot be simply ascribed to the Fowler–Nordheim oscillation [5] because there does not exist any reflected wave in the latter case.

As pointed out in [13], the asymptotic approximations of (23)–(26) and (41)–(44) agree very well with the exact Airy functions $\mathrm{Ai}(z)$, $\mathrm{Bi}(z)$, $\mathrm{Ai}'(z)$ and $\mathrm{Bi}'(z)$ except for $z \approx 0$. Therefore, a nonnegligible difference between the exact (the solid curve) and approximate (the dotted curve) TMR in figure 2 can appear only within a very small interval near the point $eV = \phi_0 - \mu$ where $z_{\mathrm{d}} \approx 0$. For this reason, the rigorous transmission coefficient of

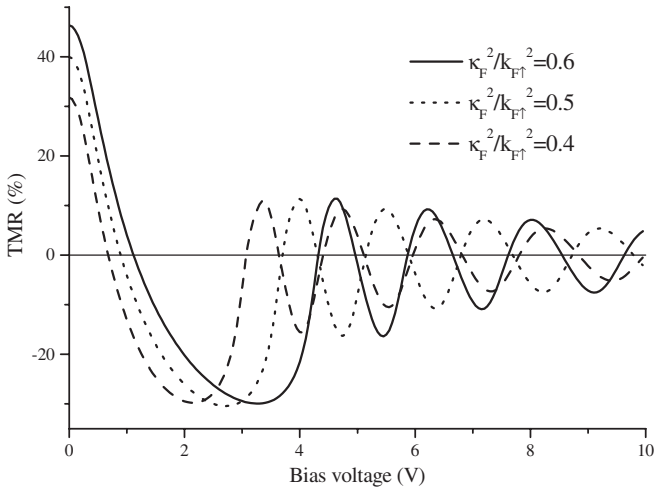

Figure 4. The curves of TMR versus bias voltage for junctions with different relative barrier heights $\kappa_F^2/k_{F\uparrow}^2 = 0.6$, 0.5 and 0.4. The other parameters are $E_{F\uparrow} = 5$ eV, $m_B/m = 1$, $k_{F\downarrow}/k_{F\uparrow} = 0.22$, $d = 20$ Å.

equation (14) and the exact Airy functions have to be used for the calculation of TMR within this small middle interval between the low- and high-bias regions.

A rectangular barrier potential at zero bias makes it convenient for us to elucidate analytically the mechanisms for the oscillation effect and the sign-change behaviour of TMR. This potential rises abruptly when it goes from the electrode into the barrier. Of course, such an abrupt step at the electrode–barrier interface is somewhat simplified. A more realistic potential for the FM/I/FM junction should take into account the rising rate of the potential between the electrode and the barrier, which will modify the potential shape into a trapezium from a rectangle, as has been successfully done by Montaigne *et al* [5]. The numerical results of [5] show that the oscillation effect and the sign-change behaviour of TMR still exist even if the potential shape is a trapezium, although the details of TMR are modified. In addition, the interface quality of FM/I/FM junctions can be improved by modern technology [14]. Therefore, the adoption of a rectangular barrier potential is reasonable for revealing the physical mechanisms of the oscillation effect and the sign-change behaviour of TMR.

3.3. Effects of the barrier height, barrier width and effective mass

We now turn to investigate and discuss the effects of the relative barrier height ($\kappa_F^2/k_{F\uparrow}^2$), barrier width ($d$) and effective mass ($m_B$) on TMR.

From the rigorous transmission coefficient and the exact Airy functions, the curves of TMR versus bias voltage are obtained numerically for various barrier parameters $\kappa_F^2/k_{F\uparrow}^2$, m_B and d; these are shown in figures 4–6, respectively.

As an overview, the TMR first drops with increasing bias voltage, changes its sign at a critical voltage V_c, and arrives at its first minimum at V_{min}. Then, it goes upwards and starts oscillating. This indicates that the sign-change behaviour in the low-bias region and the oscillation effect in the high-bias region are both general behaviours of the bias-dependent TMR in FM/I/FM junctions.

With regard to the sign-change behaviour in the low-bias region, the critical voltage V_c of the TMR increases with the relative barrier height $\kappa_F^2/k_{F\uparrow}^2$, but decreases with the electron

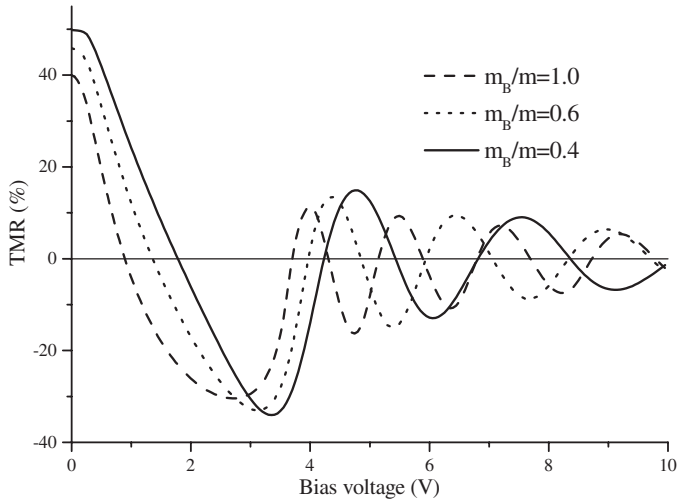

Figure 5. The curves of TMR versus bias voltage for junctions with different electron effective masses $m_B/m = 1.0$, 0.6 and 0.4. The other parameters are $E_{F\uparrow} = 5$ eV, $k_{F\downarrow}/k_{F\uparrow} = 0.22$, $d = 20$ Å, $\kappa_F^2/k_{F\uparrow}^2 = 0.5$.

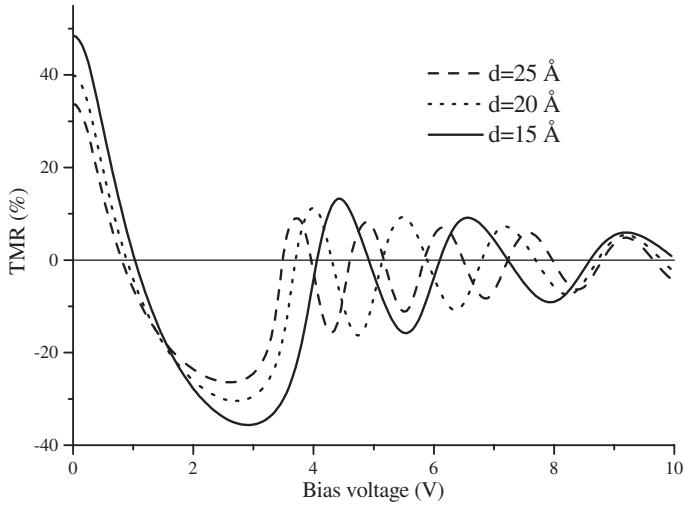

Figure 6. The curves of TMR versus bias voltage for junctions with different barrier widths $d = 25$, 20, and 15 Å. The other parameters are $E_{F\uparrow} = 5$ eV, $m_B/m = 1$, $k_{F\downarrow}/k_{F\uparrow} = 0.22$, $\kappa_F^2/k_{F\uparrow}^2 = 0.5$.

effective mass m_B or barrier width d, as shown in figures 4–6. These behaviours originate physically from the strong energy dependence of the prefactor $A(E_x^L, E_t^L, V)D(E_x^L, E_t^L, V)$ in equation (33), and especially from the quantum-coherence factor $D(E_x^L, E_t^L, V)$, as already pointed out in [3, 6–8].

The first minimum of the TMR always occurs at V_{min} in the small middle interval, which can be estimated approximately as

$$eV_{min} \approx \widetilde{\phi}_0 - \mu, \tag{61}$$

where $\widetilde{\phi}_0$ is the renormalized barrier height,

$$\widetilde{\phi}_0 = \phi_0 + E_t^L \left(\frac{m}{m_B} - 1 \right). \tag{62}$$

Equation (61) together with (62) indicates that V_{min} will increase with the barrier height ϕ_0 but decrease with the effective mass m_B, which is in agreement with the numerical results of

figures 4–6. In order to observe $V_{\min}$ and even the oscillating TMR experimentally, a junction with a lower barrier height and a larger m_B/m is needed.

Finally, we discuss the influences of m_B and d on the oscillation of TMR. As mentioned above, the oscillation behaviour arises from the function $\sin(2\gamma_d)$. When $\sin(2\gamma_d) = -1$, i.e.,

$$\frac{4}{3}d\left(\frac{2m_B}{\hbar^2}eV\right)^{1/2} = 2\pi\left(n+\frac{3}{4}\right), \qquad n = 0, 1, 2, \ldots, \tag{63}$$

the tunnelling magnetoresistance reaches its extrema. This indicates that the nth extremum appears at V_n, where

$$eV_n = \frac{9\pi^2\hbar^2}{8m_Bd^2}\left(n+\frac{3}{4}\right)^2. \tag{64}$$

Therefore, the period T of oscillation is

$$T = eV_{n+1} - eV_n = \frac{9\pi^2\hbar^2}{16}\frac{4n+5}{m_Bd^2}. \tag{65}$$

Obviously, the period T is not a constant but increases with the number n. For a fixed n, equation (65) demonstrates that the oscillating period of the TMR will reduce with the increase of either m_B or d. The analysis agrees well with the numerical results shown in figures 5 and 6, respectively.

As regards the amplitude of TMR oscillation, it decays with the applied voltage; this is because, as pointed out in [3, 6–8], the denominator $J_P(V)$ of equation (22) increases rapidly with applied voltage.

3.4. Comparison with experiments

Based on the above discussion, we will try to compare the theoretical results with experiments, qualitatively.

Three theoretical curves of TMR obtained from the rigorous transmission coefficient, equation (14), and the exact Airy functions are presented in figure 7: curve A corresponds to $\kappa_F^2/k_{F\uparrow}^2 = 0.50$ and $m_B/m = 0.4$, curve B to $\kappa_F^2/k_{F\uparrow}^2 = 0.40$ and $m_B/m = 0.6$, and curve C to $\kappa_F^2/k_{F\uparrow}^2 = 0.23$ and $m_B/m = 1.0$. Physically, they represent three different kinds of junction. Curve A stands for a junction with a high barrier and a small m_B, curve B for a junction with a lower barrier and a larger m_B, and curve C for a junction with the lowest barrier and largest m_B.

As can be seen in figure 7, curve C decreases rapidly and changes its sign with increasing bias voltage. After reaching the first minimum, it begins to bend upwards, showing a small tail until the applied voltage goes beyond the measurable range. Such features are in agreement with the TMR experiments on the Ta_2O_5-barrier junction [2]. Therefore, according to the present theory, the tail can be considered as a remnant part of the TMR oscillation within the measurable range.

Historically, for metal/insulator/metal (M/I/M) tunnel junctions, Gundlach [10] predicted theoretically that the tunnelling current can oscillate with the bias voltage. Later, in 1974, upon improving the sharpness (or abruptness) of the interface between the electrode and the barrier, Maserjian [15, 16] observed oscillation of the tunnelling current in MOS structures. Recent research [14] indicates that the interface quality can be technically improved in FM/I/FM junctions. This makes us believe that parts of the TMR oscillation other than only the tail may also be observed in future.

In contrast to curve C, curve A decreases monotonically with increasing bias voltage, but remains positive before the breakdown of the junction. This agrees with and thus can

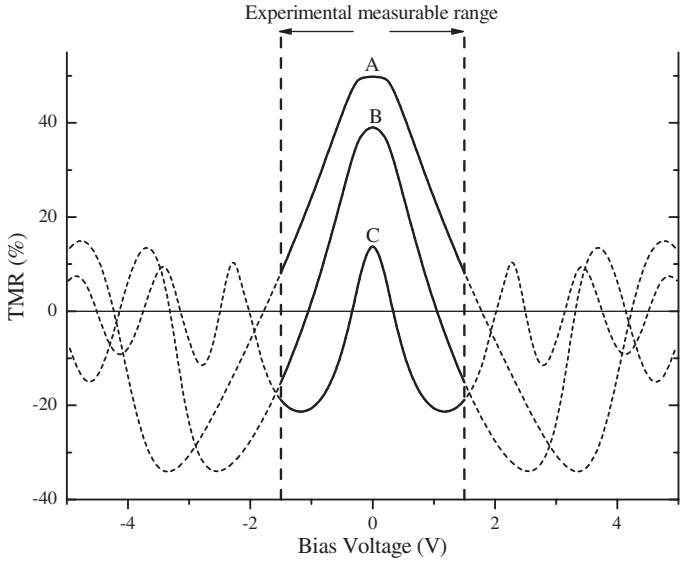

Figure 7. The curves of TMR versus bias voltage for three different kinds of junction. Curve A corresponds to $\kappa_F^2/k_{F\uparrow}^2 = 0.50$ and $m_B/m = 0.4$, curve B to $\kappa_F^2/k_{F\uparrow}^2 = 0.40$ and $m_B/m = 0.6$, and curve C to $\kappa_F^2/k_{F\uparrow}^2 = 0.23$ and $m_B/m = 1.0$. The other parameters are $E_{F\uparrow} = 5$ eV, $k_{F\downarrow}/k_{F\uparrow} = 0.22$, $d = 20$ Å.

be used to explain the experimental curve of the Al_2O_3-barrier junction. In comparison with Ta_2O_5 [17], Al_2O_3 has a much smaller m_B [18] and a larger work function [19] (i.e., a larger relative barrier height). These will lead to both a higher V_c and V_{min}, according to the analysis in the preceding subsection. That is the physical reason why the Al_2O_3-barrier junction does not exhibit any sign-change or oscillating behaviour within the experimental measurable range of the bias voltage.

In contrast to both curves A and C, curve B changes its sign but does not show a bending-up tail within the measurable range. This kind of TMR has already been observed in the ZrO_x-barrier junction [20]. Probably, it indicates that the barrier height of the ZrO_x-barrier junction is higher than that of the Ta_2O_5-barrier junction, but lower than that of the Al_2O_3-barrier junction.

The above discussions demonstrate that the free-electron-like model with parabolic bands can successfully describe the essential physics of the FM/I/FM tunnelling junctions, although it cannot describe the detail electronic structures of ferromagnetic metals.

4. Conclusions

We have presented a unified spintronic theory, which is suitable not only for low-bias tunnelling but also for high-bias tunnelling. Within this theory, the barrier potential is trapezoidal, and can be solved exactly by Airy functions.

The asymptotic expressions of Airy functions are employed to study the physical mechanisms for the sign change and the oscillation of TMR, analytically. We find that the sign-change behaviour of TMR can occur only in the low-bias region. Physically, it originates from the quantum coherence in the FM/I/FM system. In the high-bias region, the electrons near the Fermi level will enter into the conduction band of the barrier and then be reflected by the

electrode–barrier interface. As a result of the interference between the incident and reflected waves, the TMR will oscillate between positive and negative with the applied voltage in the high-bias region. The effects of the barrier height ϕ_0, barrier width d and the electron effective mass in barrier m_B on TMR have also been discussed. It turns out that a junction with a lower barrier height and a larger m_B/m is needed for TMR to show oscillation within the measurable range of bias voltage. With this reason, one can easily understand the bias dependences of TMR observed experimentally on Al_2O_3- and Ta_2O_5-barrier junctions. For the Al_2O_3-barrier junction, which has a large barrier height ϕ_0 and a very small m_B/m, the TMR will remain positive within the measurable range. In contrast, the Ta_2O_5-barrier junction has a lower barrier height ϕ_0 and a larger m_B/m, so its TMR will change in sign at a critical voltage, then bend upwards and begin to oscillate with a small tail appearing before the breakdown of the junction. These results demonstrate that the present theory is in quite good agreement with the experiments.

Finally, it is worth noting that Tsymbal and co-workers [21] find an interesting result, namely that the tunnelling magnetoresistance can be inverted at low bias via the localized states in the barrier. Physically, such localized states will lead to indirect resonant tunnelling. In order to discuss this interesting property of TMR, one needs to take further into account the resonant tunnelling arising from the localized states, in addition to the direct tunnelling considered in the present paper. This study is in progress and will be published elsewhere.

Acknowledgments

This project was supported by the State Key Project of Fundamental Research under Grant No. 001CB610602 and the National Science Foundation of China (No. 10474038).

References

[1] Jullière M 1975 *Phys. Lett.* A **54** 225
[2] Sharma M, Wang S X and Nickel J H 1999 *Phys. Rev. Lett.* **82** 616
[3] F F Li, Li Z Z, Xiao M W, Du J, Xu W and Hu A 2004 *Phys. Rev.* B **69** 054410
[4] Slonczewski J C 1989 *Phys. Rev.* B **39** 6995
[5] Montaigne F, Hehn M and Schuhl A 2001 *Phys. Rev.* B **64** 144402
[6] Li F F, Li Z Z, Xiao M W, Du J, Xu W and Hu A 2004 *J. Appl. Phys.* **95** 7243
[7] Li F F, Li Z Z, Xiao M W, Hu A and Xu W 2004 *Chin. Phys. Lett.* **21** 2271
[8] Li F F, Li Z Z and Xiao M W 2005 *Chin. Phys.* **14** 1025
[9] Burstein E and Lundqvist S 1969 *Tunneling Phenomena in Solids* (New York: Plenum) p 31
[10] Gundlach K H 1966 *Solid-State Electron.* **9** 949
[11] Duke C B 1969 *Tunneling in Solids* (New York: Academic)
[12] Abramowitz M and Stegun I A 1965 *Handbook of Mathematical Functions* (New York: Dover) pp 446–52
[13] Merzbacher E 1998 *Quantum Mechanics* 3rd edn (New York: Wiley) p 118
[14] Shen F, Zhu T, Xiang X H, Xiao J Q, Voelkl E and Zhang Z 2003 *Appl. Phys. Lett.* **83** 5482
[15] Maserjian J 1974 *J. Vac. Sci. Technol.* **6** 996
[16] Wolf E L 1985 *Principles of Electron Tunneling Spectroscopy* (New York: Oxford University Press) p 64
[17] Rottländer P, Hehn M, Lenoble O and Schuhl A 2001 *Appl. Phys. Lett.* **78** 3274
[18] Gundlach K H and Holzl J 1971 *Surf. Sci.* **27** 125
[19] Samsonov G V 1982 *The Oxide Handbook* (New York: IFI/Plenum)
[20] Sheng W T, Wang W G, Xiang X H, Shen F, Li F F, Zhu T, Zhang Z, Li Z Z, Du J, Hu A and Xiao J Q 2004 *J. Electron. Mater.* **33** 1274
[21] Tsymbal E Y, Sokolov A, Sabirianov I F and Doudin B 2003 *Phys. Rev. Lett.* **90** 186602